Synergetic modulation of mobility and thermal conductivity in $(Bi,Sb)_2Te_3$ towards high thermoelectric performance

Yu Pan, [a,b] Yang Qiu, [c] Ian Witting, [d] Liguo Zhang, [b] Chenguang Fu, [b] Jing-Wei Li, [a] Yi Huang, [c] Fu-Hua Sun, [a] Jiaqing He, [c] G. Jeffrey Snyder, [d] Claudia Felser, [b] Jing-Feng Li*[a]

[a] *State Key Laboratory of New Ceramics and Fine Processing, School of Materials Science and Engineering, Tsinghua University, 100084 Beijing, P. R. China.*

[b] *Max Planck Institute for Chemical Physics of Solids, Nöthnitzer Str. 40, 01187, Dresden, Germany.*

[c] *Department of Physics, South University of Science and Technology of China, Shenzhen 518055, China.*

[d] *Department of Materials Science and Engineering, Northwestern University, Evanston, IL 60208, USA.*

**Corresponding author.*
J.-F. Li, Tel.: +86 10 62784845
E-mail address: jingfeng@mail.tsinghua.edu.cn

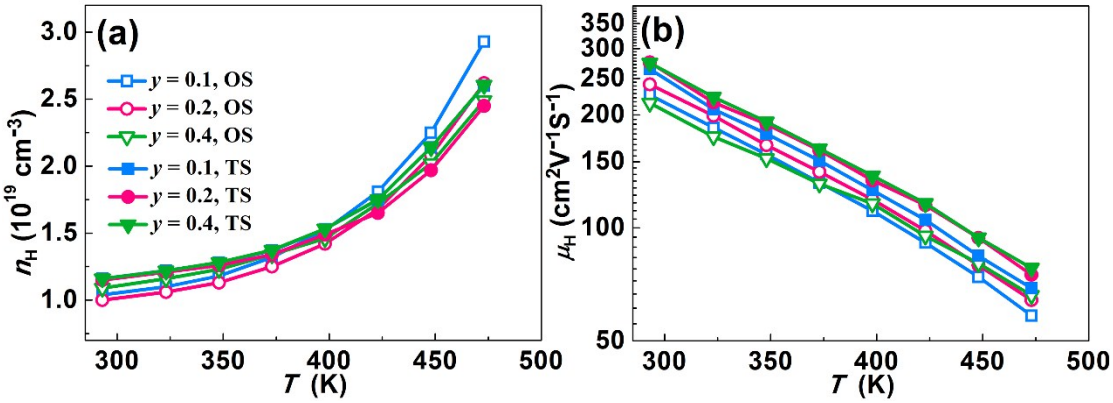

Fig. S1 (a) Hall carrier concentration and (b) Hall carrier mobility of one-step and two-step sintering samples.

All the samples with different amounts of Te show almost equal Hall carrier concentrations at around 1×10^{19} cm^{-3}. Comparing to the one-step and two-step sintered samples, Hall carrier mobility was enhanced for all the $Bi_{0.5}Sb_{1.5}Te_{3+y}$ samples.

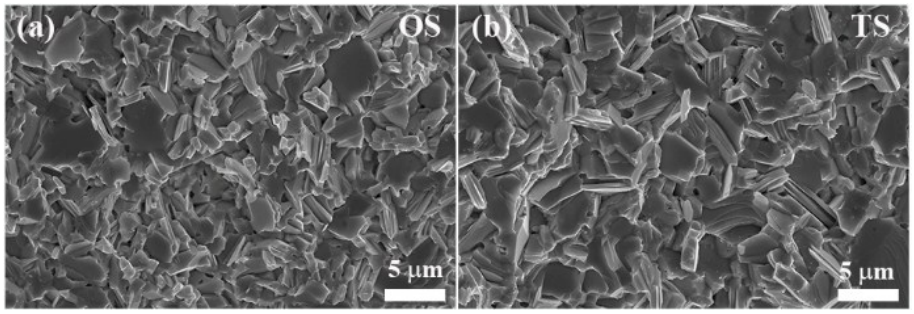

Fig. S2 SEM images of the fractured surfaces of $Bi_{0.5}Sb_{1.5}Te_{3.2}$ OS and TS samples.

The fractured surfaces of both OS and TS samples are shown in **Fig. S2**. The SEM images illustrate no obvious texture degree of both OS and TS samples. Nevertheless, the grain size of TS sample seems larger than the OS sample, which can be one of the reasons for the increased mobility due to reduced grain boundary scattering.

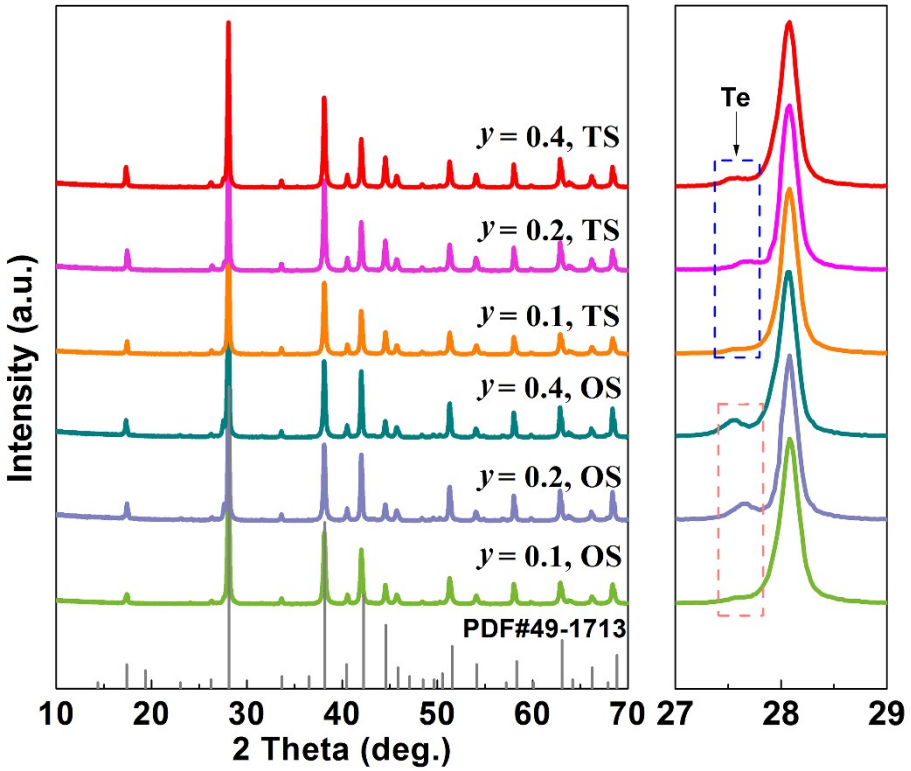

Fig. S3 XRD patterns of the $Bi_{0.5}Sb_{1.5}Te_{3+y}$ samples produced by one-step (OS) and two-step (TS) sintering process.

XRD patterns in **Fig. S3** show that the Te peak shrinks after the second step sintering, indicating that Te is expelled out during the second-step sintering process. Since the excess amount of Te is small, we didn't see extruded Te (or Te-$(Bi,Sb)_2Te_3$ eutectic phase) bulks outside of the die, instead, they are found at the cylindrical surface of the punch (on the side close to the sample) between the punch and the graphite paper. The residual amount of Te is ~5 % after the second step sintering, which hardly has an effect on the thermoelectric performance of $(Bi,Sb)_2Te_3$.

On the other hand, both OS and TS samples show negligible texture degree according to the orientation factors (*F* number) based on the XRD results. *F* numbers are calculated according to the following equations:

$$F = \frac{P - P_0}{1 - P_0}$$

$$P_0 = \frac{I_0(00l)}{\sum I_0(hkl)}, \quad P = \frac{I(00l)}{\sum I(hkl)}$$

where P and P_0 are the integrated intensities of all ($00l$) planes to the intensities of all (hkl) planes for preferentially and randomly oriented samples. Here (0,0,6), (0,0,9),

(0,0,15) and (0,0,18) are used to calculate $I(00l)$. The calculated F values of OS and TS samples are ~0.052 and 0.087, respectively, using the XRD pattern of powder sample as a reference. The small increase of F number may indicate the slightly enhanced texture degree of the TS sample compared to the OS sample. However, since these F numbers are too small to declare a texture degree. This is reasonable as the second-step sintering is conducted in the die with the same diameter of the sample wherein samples do not go through a hot forge process.

To further compare the texture degree of OS and TS samples, bulk XRD of the in-plane (perpendicular to the SPS pressure) and cross-plane (parallel to the SPS pressure) directions are conducted for both OS and TS samples. As shown in **Fig. S6**, no obvious differences are found between the in-plane and cross-plane direction. This may rule out the enhanced texture degree as a reason for the increase of mobility.

Table S1 Densities of the OS and TS $Bi_{0.5}Sb_{1.5}Te_{3+y}$ samples.

Density (g/cm^3)	$y = 0.1$	$y = 0.2$	$y = 0.4$
OS	6.486 (95.4 %)	6.471 (95.2 %)	6.419 (94.4 %)
TS	6.473 (95.2 %)	6.383 (93.9 %)	6.340 (93.2 %)

Although Te phase was extruded out during the second-step sintering and black holes show up in the BSE images, there is little change of the densities, as shown in **Table S1**. The reason is probably due to the size distribution of the pores, for example, in the OS sample there are many smaller pores while in the TS samples the pores become larger, but the total numbers of the pores in the TS samples become fewer. This can also be seen from the SEM images shown in **Fig. S2**.

The lattice parameters are calculated based on the XRD patterns, which are nearly the same for OS and TS samples, as shown in **Table S2** below.

Table S2 Lattice parameters of the OS and TS samples.

Lattice parameters (nm)	$y = 0.1$, OS	$y = 0.1$, TS	$y = 0.2$, OS	$y = 0.2$, TS	$y = 0.4$, OS	$y = 0.4$, TS
a	0.42967	0.42969	0.42988	0.42970	0.42975	0.42978
b	0.42967	0.42969	0.42988	0.42970	0.42975	0.42978
c	3.04945	3.04929	3.04978	3.05092	3.04939	3.04914

For the $y = 0$ sample without excess Te, the mobility still increased after the second-step sintering process, demonstrating the effectiveness of two-step sintering technique for mobility enhancement. While the lattice thermal conductivity increased a little for $y = 0$ samples. In consequence, the overall zT show no difference between the OS and TS samples, indicating that excess Te is necessary for the reduction of thermal conductivity and hence zT improvement, as shown in **Fig. S4**. In other words, the second-step liquid phase sintering based on the extrusion of molten Te is significant for the reduction of thermal conductivity.

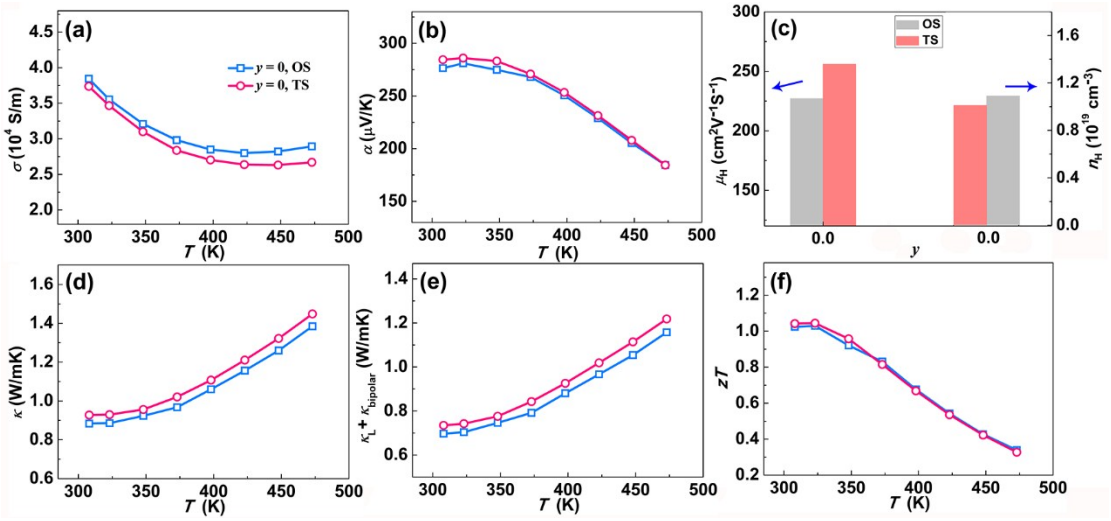

Fig. S4 Thermoelectric transport properties of y =0 ($Bi_{0.5}Sb_{1.5}Te_3$) OS and TS samples, (a) electrical conductivity, (b) Seebeck coefficient, (c) mobility and carrier concentration, (d) thermal conductivity, (e) lattice and bipolar thermal conductivity and (f) zT values.

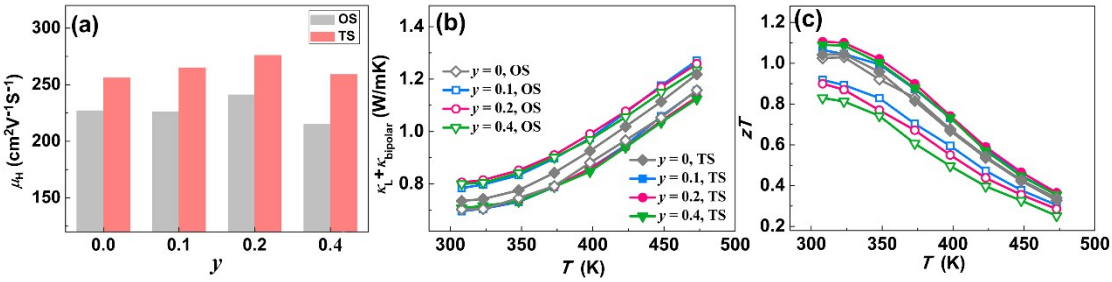

Fig. S5 Comparison of (a) mobility, (b) lattice and bipolar thermal conductivity and (c) zT values of the $Bi_{0.5}Sb_{1.5}Te_{3+y}$ (y = 0, 0.1, 0.2, 0.4) samples.

To better illustrate the role of the removal of Te, **Fig. S5** gives a comparison of the mobility, lattice and bipolar thermal conductivity and zT values for the y = 0 and y > 0 samples.

Firstly, excess Te as well as their removal has little effect on the mobility. As shown in **Fig. S5**(a), the mobility still shows an increase for the TS sample compared to the OS sample for y = 0, demonstrating that the enhancement of mobility is not due to the removal of Te. This can also be figured out by realizing that all the OS samples have almost the same mobility values regardless of the y values.

Secondly, the decrease of the lattice thermal conductivity (κ_L) is related to the removal of Te, but noteworthy, it is not totally due to the removal of Te. As shown in **Fig. S5**(b), y > 0 TS sample has almost the same κ_L as y = 0 OS sample, but the κ_L of y > 0 TS sample is much higher that the y = 0 OS sample, indicating that the removal of Te decreased the κ_L. While the reasons why the reduction of κ_L do not fully stems from the removal of Te can be explained by the following analysis: (1) simply conduct the two-step sintering without excess Te results in an increase of κ_L; (2) excess Te themselves increase the κ_L, as y > 0 OS samples have higher κ_L values than y = 0 OS

samples; (3) supposing that excess Te are added and they would not be extruded out during the second-step sintering process, then the TS sample with excess Te would be much higher than the OS sample, because both condition (1) and (2) contributes to the increase of κ_L (simply put, (3)=(1)+(2)). At this stage, we move back to our present case, where the excess Te has been expelled out after the TS process. If the reduction of κ_L all comes from the removal of Te, then the final κ_L of $y > 0$ TS sample should be higher than the $y = 0$ OS sample due to condition (1) as well as the residual Te (though very small amount, ~ 5 %). But the results show that the final κ_L of $y > 0$ TS sample is almost the same as the $y = 0$ OS sample, indicating that there are other reasons for the decrease of κ_L, for example, Sb-rich inhomogeneities as detected by the TEM.

At last, y > 0 TS sample show the best thermoelectric performance, as shown in **Fig. S5**(c), indicating that the second-liquid sintering process is essential for the zT enhancement.

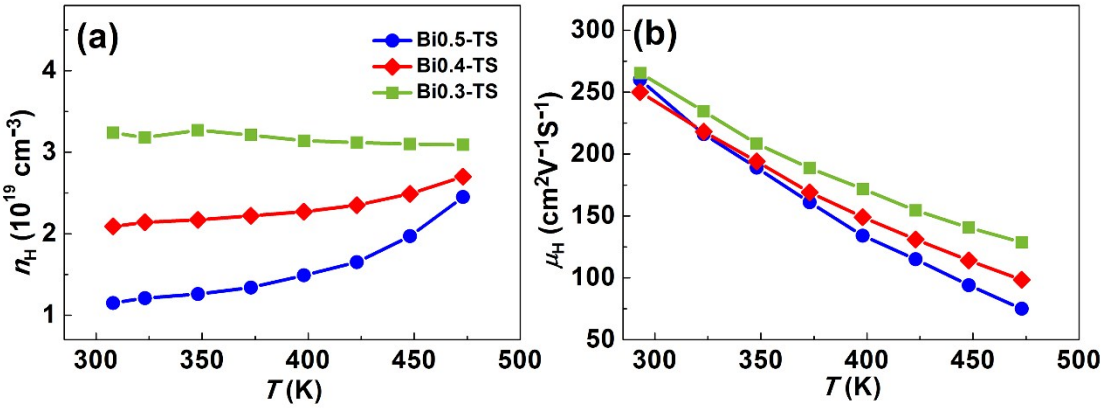

Fig. S6 (a) Hall carrier concentration and (b) Hall carrier mobility of two-step sintered $Bi_xSb_{2-x}Te_3$ samples.

By changing the Bi/Sb ratio from 0.5/1.5 to 0.4/1.6 and 0.3/1.7, the Hall carrier concentration increased from ~1×10^{19} cm^{-3} to ~2×10^{19} cm^{-3} and ~3×10^{19} cm^{-3}. Moreover, the Hall carrier mobility was also enhanced due to the suppression of intrinsic excitation.

Cycling measurements of thermoelectric transport properties were performed for the sample with the best thermoelectric performance (two-step sintered $Bi_{0.4}Sb_{1.6}Te_3$). As shown in **Fig. S7**, no hysteresis was found between heating and cooling, indicating a phase stability of the present samples.

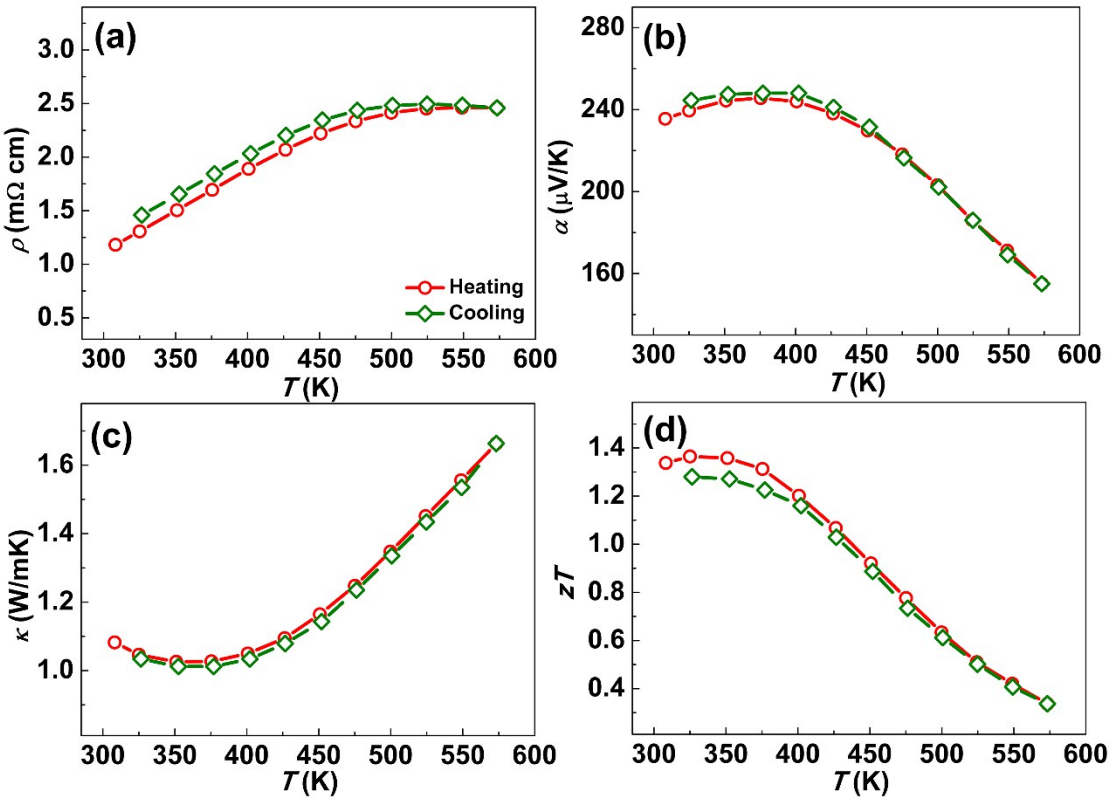

Fig. S7 Heating and cooling measurements of (a) resistivity, (b) Seebeck coefficient, (c) thermal conductivity, and (d) zT values for two-step sintered $Bi_{0.4}Sb_{1.6}Te_3$.

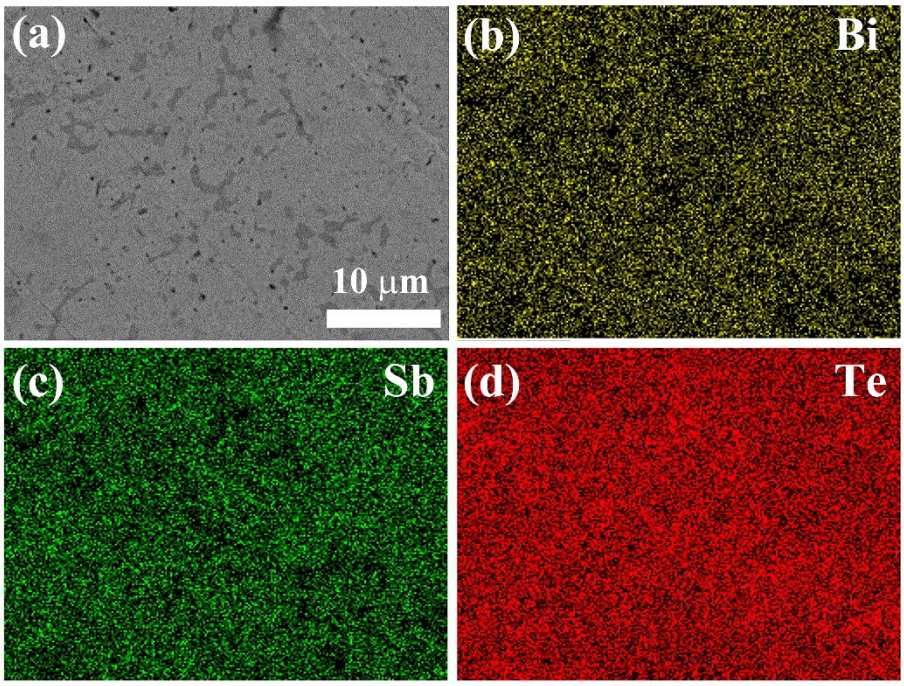

Fig. S8 Te existence and distribution in the samples produced by one-step sintering process demonstrated by SEM and EDS mapping. (a) Microstructure in back scattering electron (BSE) mode of scanning electron microscopy (SEM). (b)-(d) EDS mapping results of Bi, Sb and Te, respectively.

SEM and EDS results demonstrated that the second phase is Te. As shown in **Fig. S8**, both Bi and Sb are insufficient at the areas corresponding to the black zones in **Fig. S8**(a), while Te seems much more homogenous, indicating that the second phase shown in BSE image is Te. These Te phases are few micrometers.

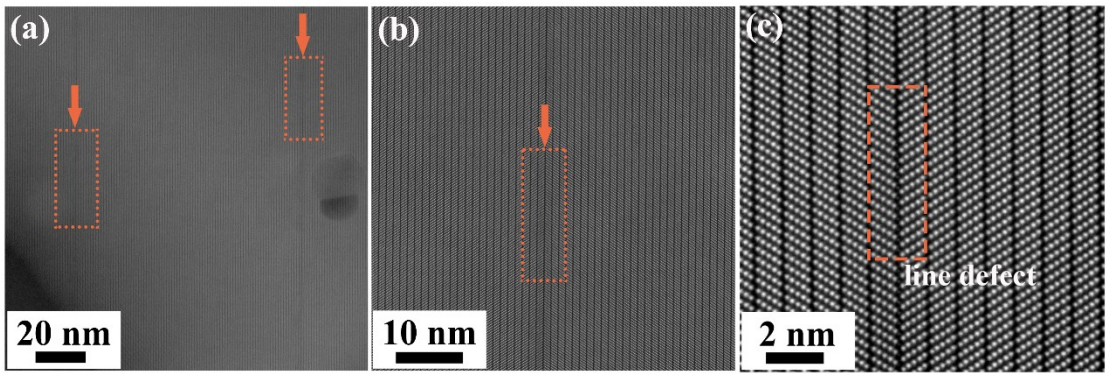

Fig. S9 High resolution HAADF-STEM of $(Bi,Sb)_2Te_3$ showing a five-layer structure and the reversal of basal plane stacking at the Te(1) layers. The orange arrows and rectangulars are used to guide the eye. The defect cross the whole grain finish at the end of the grain boundary.

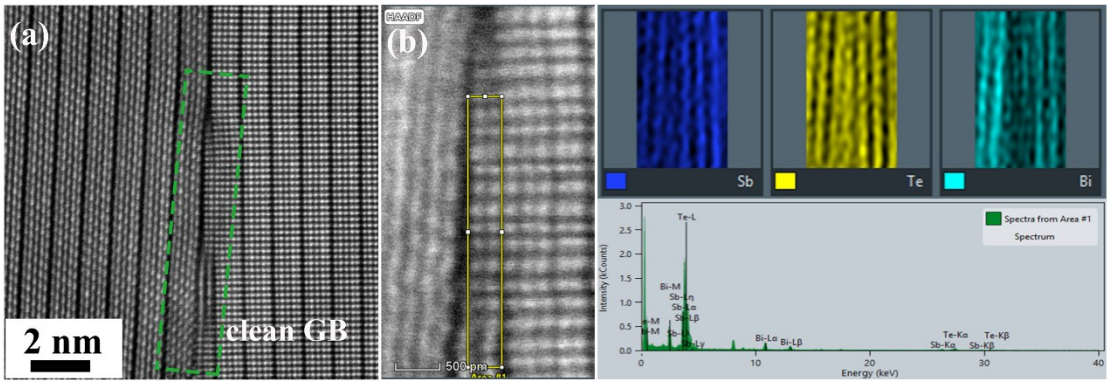

Fig. S10 High resolution HAADF-STEM of $(Bi,Sb)_2Te_3$ showing (a) grain boundary dislocations and (b) lattice resolved EDX mapping results. No Te or other second phase was found at the interface in the TS sample.

Two band modeling

With two kinds of charge carrier contribute to the conduction, the carrier concentration, electrical conductivity, Seebeck coefficient and thermal conductivity can be expressed as the following equations:[1]

$$n = n_e + n_p$$

$$\sigma = \sigma_e + \sigma_p = e(\mu_e n_e + \mu_p n_p)$$

$$\alpha = \frac{\alpha_e \sigma_e + \alpha_p \sigma_p}{\sigma_e + \sigma_p}$$

$$\kappa = \kappa_L + (L_e\sigma_e T) + (L_p\sigma_p T) + \frac{\sigma_e\sigma_p(\alpha_p - \alpha_e)^2}{\sigma_e + \sigma_p}T$$

Where the subscripts e and p present electrons and holes, respectively. For either electrons or holes, based on a single parabolic band and acoustic scattering mechanism for simplicity, the transport properties can be written as:

$$\alpha_i = \frac{k_B}{e}\left(\frac{2F_{i,1}}{F_{i,\,0}} - n_i\right)$$

$$n_i = 4\pi\frac{k_B}{e}\left(\frac{2m_i^* k_B T}{h^2}\right)^{3/2}F_{i,1/2}$$

$$\mu_{i,H} = \mu_{i,0}\frac{F_{i,\,-1/2}}{2F_{i,\,0}}$$

$$L_i = \left(\frac{k_B}{e}\right)^2\left(\frac{3F_{i,0}F_{i,2} - 4F_{i,1}^2}{F_{i,0}^2}\right)$$

Where $F_{i,j}$ in the Fermi integrals of charge carriers,

$$F_{i,j}(\eta_i) = \int_0^\infty \frac{\varepsilon^j d\varepsilon}{1 + exp(\varepsilon - \eta_i)}$$

In which subscript i=electrons, holes. Herein define $\mu_{i,w} = \mu_{i,0}\left(\frac{m_i^*}{m_e}\right)^{3/2}$ as weighed mobility,[2] as such two variables are combined into one.

In the present work, holes are the major charge carriers, define $\eta_e = \eta_p - \frac{\Delta}{k_B T}$, where Δ is the energy difference between conduction band and valence band. All the transport properties can be solved out when the Fermi level and weighed mobilities are determined. Firstly, conduction at room temperature is supposed to be contributed only by holes, which has also been confirmed by other groups. In this way, we can easily get the Fermi level and weighed mobility at room temperature. Secondly, by taking a linear variation of Fermi level and a $T^{-1.5}$ decreasing law for mobility, temperature dependent transport properties can be obtained. Here the modeling values are shown in **Table S3**.

Table S3 Parameters for two band modeling.

T (K)	Δ (eV)	η_p	$\mu_{p,w}$ (cm^2/Vs)	$\mu_{e,w}$ (cm^2/Vs)	n_p (10^{19} cm^{-3})	n_e (10^{17} cm^{-3})	L_p	L_e
308	0.25	-0.35	525	160	2.10	0.91	1.59	1.49
323	0.25	-0.45	467	130	2.16	1.70	1.58	1.49

348	0.25	-0.57	405	110	2.17	3.16	1.57	1.49
373	0.25	-0.67	351	95	2.19	5.41	1.57	1.49
398	0.25	-0.77	305	92	2.21	8.81	1.56	1.49
423	0.25	-0.86	270	90	2.23	13.42	1.55	1.49

Reference

1. Rowe DM. Material, preparation, and charaterization in thermoelectrics. *CRC Press* 2012.
2. Kang SD, Pöhls J-H, Aydemir U, Qiu P, Stoumpos CC, Hanus R*, et al.* Enhanced stability and thermoelectric figure-of-merit in copper selenide by lithium doping. *Mate. Today Phys.* 2017, **1:** 7-13.